Electromagnetic interference shielding efficiency of MnO_2 nanorod doped polyaniline film

Materials Research Express

Electromagnetic interference shielding efficiency of MnO$_2$ nanorod doped polyaniline film

Pritom J Bora[1], **K J Vinoy**[2], **Praveen C Ramamurthy**[1,3] **and Giridhar Madras**[1]

1   Interdisciplinary Centre for Energy Research (ICER), Indian Institute of Science, Bangalore-560012, India
2   Department of Electricals and Communications Engineering, Indian Institute of Science, Bangalore-560012, India
3   Department of Materials Engineering, Indian Institute of Science, Bangalore-560012, India

E-mail: onegroupb203@gmail.com

Abstract

The polymer nanocomposite thin film is of interest due to many advantages for electromagnetic interference (EMI) shielding. In this work, low temperature ($-30 \pm 2\,°C$) *in situ* synthesized polyaniline (PANI)–MnO$_2$ nanorod composite (PMN) were solution processed, followed by acid vapor treatment for preparing free standing films and EMI shielding effectiveness (SE) were investigated in the frequency range i.e. X-band (8.2–12.4 GHz) and Ku-band (12.4–18 GHz). As prepared PMN film ($169 \pm 2\ \mu m$) shows most effective EMI SE ~ 35 dB (EMI shielding due to absorption, SE$_A$ ~ 24 dB and EMI shielding due to reflection SE$_R$ ~ 11 dB) in the X-band which was observed to be ~39 dB (SE$_A$ ~ 29 dB and SE$_R$ ~ 10 dB) in the Ku-band. The variations of conductivity, penetration depth, EM attenuation constant of the PMN film in the X-band and Ku-band were also investigated along with dielectric study.

1. Introduction

The rapid increase in high frequency (8–18 GHz) based electrical/electronic devices has resulted in electromagnetic interference (EMI). EMI pollution becomes a serious issue for modern telecommunications, robotics, unmanned vehicles as well as microwave engineering [1–3]. The demand of polymeric shielding materials is increasing as these are more flexible and lightweight compared to metals. Further, these materials are less prove to corrosion, can be easily coated onto any substrate (especially organic nanoelectronic devices) and relatively inexpensive [1–5]. Mechanistically, EMI shielding takes place mainly due to reflection and absorption [1]. However, the design of high EMI shielding due to absorption material/film is important. Intrinsic conducting polymer (ICP) and its composites especially polyaniline (PANI) have been proposed as excellent EMI shielding materials [6–8]. PANI-carbon nanotube (CNT)/graphene composite [9], PANI-silicon rubber composites [10], PANI-silver nanowire composites [11] etc are found to be useful for EMI shielding applications. The emaraldine salt (ES) form of PANI powder can be used as a filler in the polymer matrix for preparing EMI shielding polymeric sheets [12]. However, filler content should be high and thickness should be large for EMI shielding effectiveness (30 dB).

According to the literature [12], the most effective ~26.7 dB EMI SE at 8.8 GHz can be achieved for 1.9 mm thick PU-PANI (PU: aniline ratio was 1:1) composite sheet with an average SE of ~10 dB in the X-band (8.2–12.4 GHz). Similarly, Saini *et al* [13] reported ~24 dB EMI SE of PANI-multiwall CNT dispersed PS (30 wt%) composite (1 mm) in Ku-band (12.4–18 GHz). Further, they reported that by increasing thickness to 2 mm, 40–45 dB EMI SE can be reached in the same frequency range. Hong *et al* [14] investigated the EMI SE of PANI ES film in the wide frequency range (50 MHz–13.5 GHz). They reported PANI ES (90 μm) film shows ~18 dB EMI SE (EMI SE due to absorption, SE$_A$ ~ 12 dB and EMI SE due to reflection, SE$_R$ ~ 6 dB).

The factors that influence EMI shielding (far field source) are complex permittivity, complex permeability, conductivity, EM attenuation loss and skin depth of the materials [1, 2]. The external factor includes thickness of the shield and source to shield distance [2]. In case of conducting polymer film, EMI shielding depends on both ε' and ε'' i.e. absolute value of complex permittivity. At high frequency (GHz), electrical loss plays a key role and high dielectric loss containing metal oxides based composites are of interest for EMI shielding due to absorption
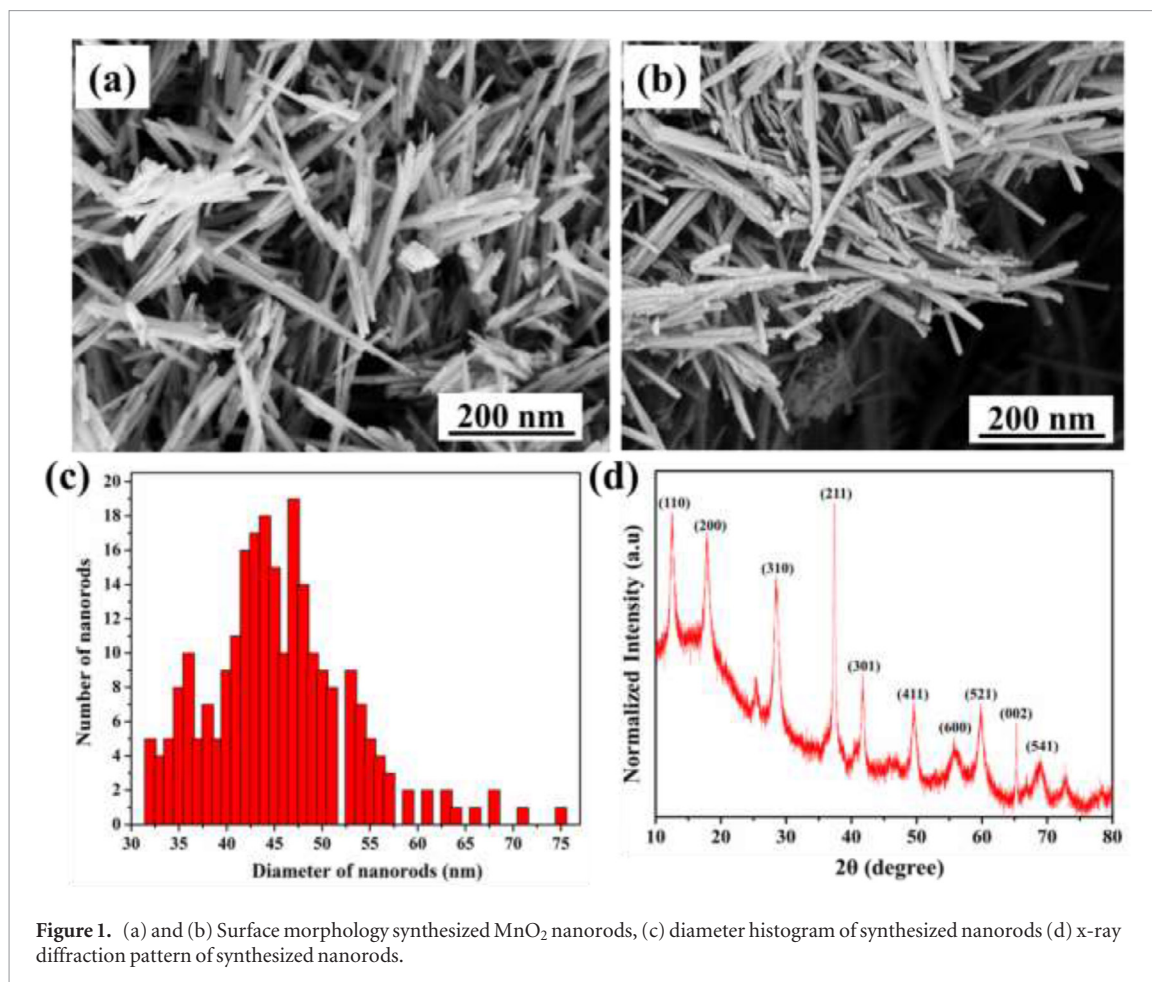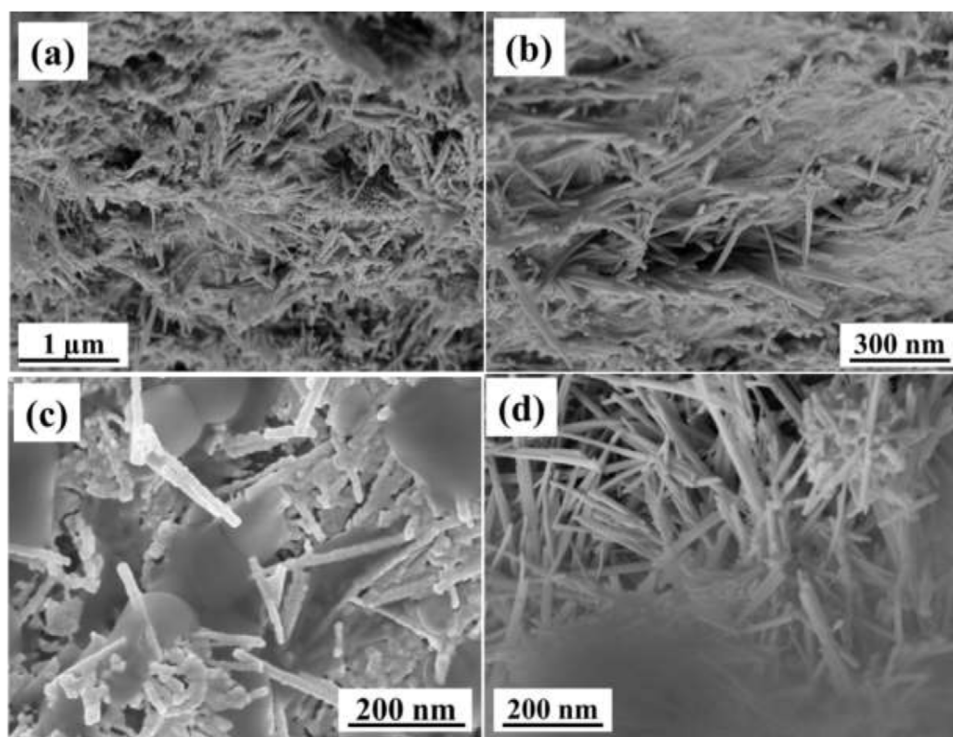
Figure 1. (a) and (b) Surface morphology synthesized MnO_2 nanorods, (c) diameter histogram of synthesized nanorods (d) x-ray diffraction pattern of synthesized nanorods.

[15]. Anisotropic nanoparticles, especially, rod shape metal oxides are reported as most suitable for microwave absorption. The microwave antenna absorption mechanism is proposed for nano tree/fibre and rod shaped metal oxides [15–17].

Among the metal oxides, manganese dioxide (MnO_2) is known for catalysis, antioxidant and antibacterial properties along with supercapacitor application [18–22]. However, recently, MnO_2 has drawn attraction for microwave absorption due to many advantages such as natural abundance, easy synthesis, thermal stability and inexpensive precursors [23, 24]. Among the various crystalline states of MnO_2 ($\alpha, \beta, \gamma, \varepsilon$), α-MnO_2 is reported as a better microwave absorber (especially anisotropic α-MnO_2) [24]. Song *et al* [25] reported that 30 wt% β-MnO_2 nanorod containing paraffin wax can show a reflection loss (RL) up to −10 dB (~11 GHz) at 2.75 mm thickness. According to the literature [26], the low temperature annealed α-MnO_2 nanorods has better microwave absorption capability. They reported ~ −13.5 dB RL (18 GHz) paraffin-MnO_2 nanocomposite (thickness 2 mm, 30 wt% MnO_2). Lv *et al* [16] studied the paraffin/β-MnO_2 nanorods composite, paraffin-Fe coated β-MnO_2 nanorods and paraffin-graphene Fe coated β-MnO_2 nanorods composites for microwave absorption [16]. According to their results, the latter is promising that shows −15 dB RL at 12 GHz for a thickness of 3 mm (paraffin:graphene-Fe-MnO_2 nanorods is 1:1).

The room temperature MnO_2 polymerized aniline shows a promising conductivity of PANI ES which can be further increased by controlling temperature/crystallinity [27]. The low temperature ($−30 \pm 2$ °C) synthesis of PANI is known for high molecular weight, high crystallinity and higher conductivity [28]. The *in situ* synthesized PANI-MnO_2 nanocomposite has been reported for supercapacitor application [29]. Gemeay *et al* [30] reported the *in situ* synthesis of PANI-MnO_2 nanorod composite. Bisanha *et al* [31] studied the reaction conditions of PANI-MnO_2 nanocomposite and showed that low temperature synthesis results in uniform, homogeneous and thicker coating of PANI over MnO_2 nanoparticles.

Hence, PANI-MnO_2 nanorod composite film can be expected as a novel EMI shielding coating material. The objective of the present work was to study the EMI shielding behaviour of *in situ* synthesized PANI-MnO_2 nanorod composite film. The EMI SE was investigated in the X and Ku-band and the effect of various parameters that influence the shielding was determined.
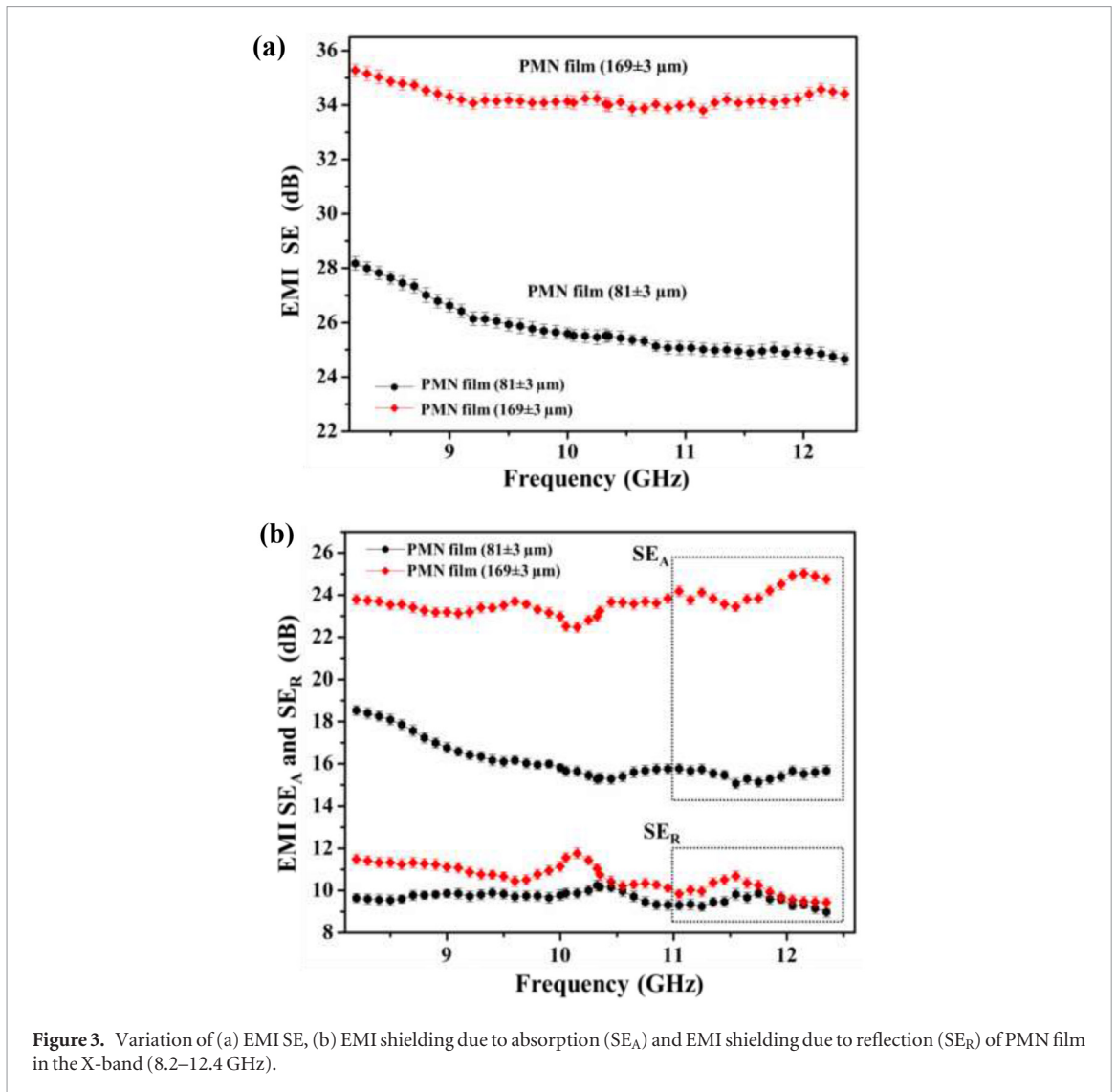
Figure 2. (a)–(c) Cross sectional surface morphology of PMN film in different regions, (d) cross sectional edge morphology of PMN film.

2. Experimental

The MnO_2 nanorods were synthesized according to the procedure described in the literature [26]. The *in situ* synthesis of PANI-MnO_2 hybrid nanocomposite was performed at $-30 \pm 2\,°C$ under nitrogen. In the typical synthesis, 0.25 g of the as-synthesized MnO_2 nanorods were dispersed in 50 ml DI water at $-30 \pm 2\,°C$. The freezing point was controlled by adding 6 M LiCl. In the second step, 1 ml double distilled aniline was added to the 50 ml 1 M HCl solution (also containing 6 M LiCl) at $-30 \pm 2\,°C$ under stirring. The molecular weight of PANI obtained was ~912 000 [28]. This solution was slowly added to the pre-cooled MnO_2 nanorods dispersed solution and the reaction was allowed to proceed for another 6 h at $-30 \pm 2\,°C$. After 6 h, obtained dark green product was filtered and washed several times with ethanol and DI water and deprotonated by stirring in 4 wt.% NH_4OH for 8 h. The obtained composite was again washed with DI water and ethanol repeatedly and was vacuum dried at 50 °C for 12 h. The freestanding films of as synthesized composite were prepared by solution processing. Optimally, 3 wt.% of synthesized PANI-MnO_2 powder was added very slowly to the dimethyl-propylene urea (DMPU) solvent under stirring and further stirred for 12 h. The resulting solution was poured on to glass moulds and placed in an oven under a dynamic vacuum of 400 mm Hg at 65 °C for 12 h. Thus resulting film was again treated with 1 M HCl solution (vapour) for 72 h to achieve stable conductivity. The prepared films were named as PMN film.

2.1. Characterizations

Surface morphologies of the synthesized materials and films were analysed using high resolution FESEM (Carl Zeiss) of the sample coated over carbon tape, sputter coated with gold. The thicknesses of the sample films were measured using Dektek. The x-ray diffraction pattern of the synthesized materials were studied by using Rigaku x-ray diffractometer using Cu K_{α} radiation ($\lambda = 1.540\,598\,Å$) in scattering range (2θ) of 10–80°. The EMI SE of the prepared PMN film was measured by waveguide method using a vector network analyser (VNA, Agilent NS201). A full standard two port calibration (thru-reflect-line, TRL) was performed for the X-band (8.2–12.4 GHz) and Ku-band (12.4–18 GHz). The sample films were clamped in between two waveguides and complex S-parameters ($S_{21}, S_{11}, S_{12}, S_{22}$) and, hence, reflectance (R), transmittance (T) and absorbance (A) were measured. The measurements of sample films were carried out three times. The complex permittivity ($\varepsilon^* = \varepsilon' - i\varepsilon''$) of the PMN film was determined from the obtained S-parameters [32].

Figure 3. Variation of (a) EMI SE, (b) EMI shielding due to absorption (SE$_A$) and EMI shielding due to reflection (SE$_R$) of PMN film in the X-band (8.2–12.4 GHz).

3. Results and discussion

3.1. Surface morphology and XRD of synthesized PMN composite and film

The surface morphology and XRD pattern of the as synthesized MnO_2 nanorods is shown in the figures 1(a) and (b), respectively. Obtained morphology shows the formation of MnO_2 nanorods having average diameter range 40–50 nm and the average length ~1.2 μm. The x-ray diffraction (figure 1(d)) pattern of as synthesized MnO_2 nanorods suggests the formation α-MnO_2 phase [16, 26]. Figures 2(a)–(c) shows the surface morphology of the prepared PMN film. As aniline was polymerized by α-MnO_2 nanorods itself, hence, grafting of PANI takes place over the MnO_2 nanorods and thus can improve the effective permittivity of the medium.

3.2. EMI SE and shielding mechanism of PMN film

The EMI shielding property of a material is measured in terms of shielding effectiveness (SE) and 30 dB EMI SE corresponds to 99.99% shielding [1, 2]. In terms of power, the EMI shielding refers logarithmic output power (P_o) to input power (P_i) and it takes place due to absorption, reflections and multiple reflections (correction factor), i.e. [2],

$$SE(dB) = -10 \log(P_o/P_i) = SE_A + SE_R + SE_M \tag{1}$$

SE$_A$, SE$_R$ and SE$_M$ represents the EMI shielding due to absorption, reflections and multiple reflections respectively [1, 2]. The EMI SE can be directly obtained from the S-parameters, i.e. EMI SE (dB) $= |S_{21}|$ [33]. Here, S_{21} corresponds to the power transmitted from port 2 to port 1 of the VNA. The SE$_A$, SE$_R$ and SE$_M$ can be obtained from the measured transmittance (T), reflectance (R) and absorbance (A) using following relations [19, 34],

$$SE_R(dB) = -10 \log(1 - R) \tag{2}$$

$$SE_A(dB) = -10 \log(1 - A_{eff}) = -10 \log \frac{T}{1 - R} \tag{3}$$
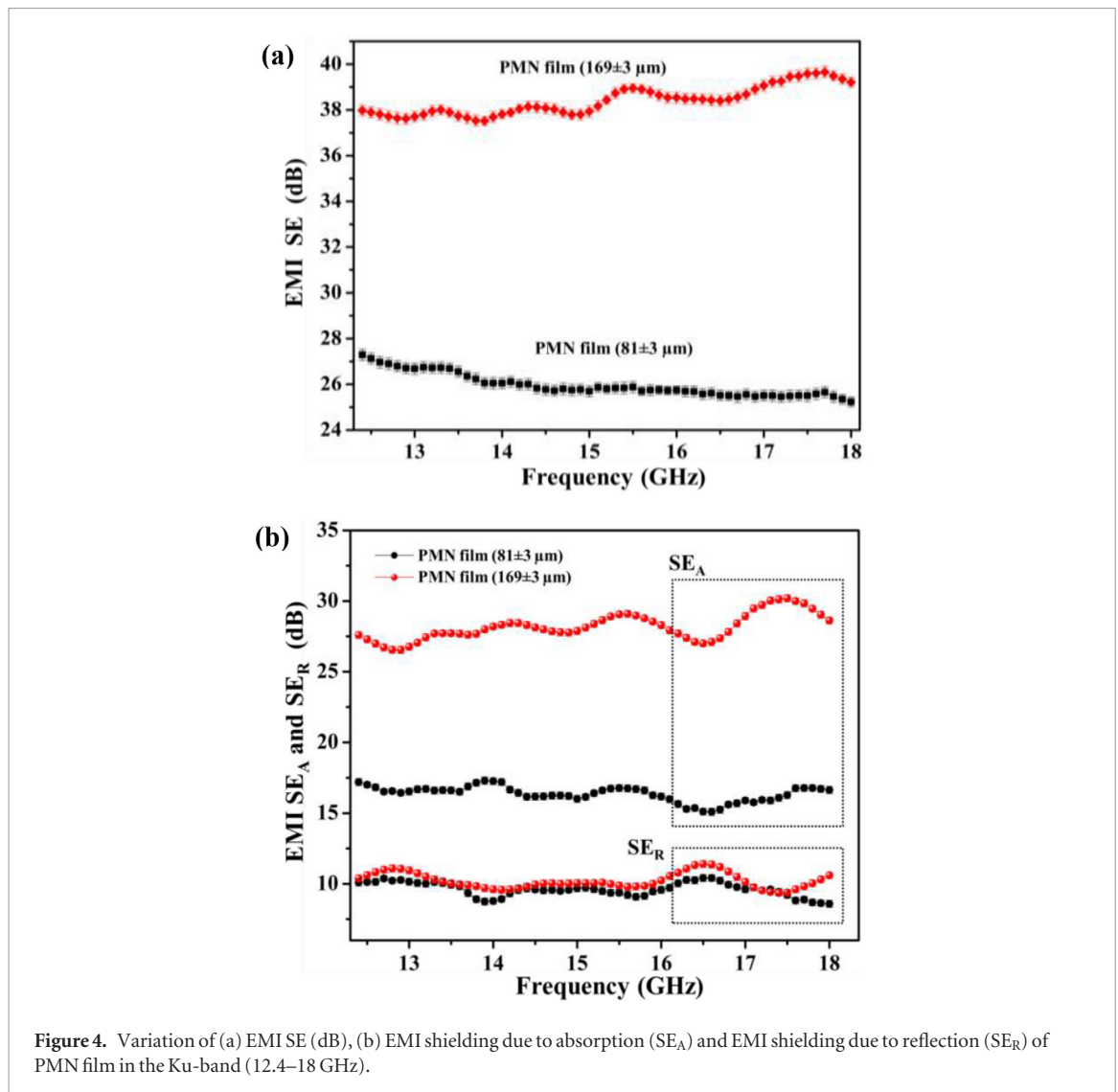
Figure 4. Variation of (a) EMI SE (dB), (b) EMI shielding due to absorption (SE$_A$) and EMI shielding due to reflection (SE$_R$) of PMN film in the Ku-band (12.4–18 GHz).

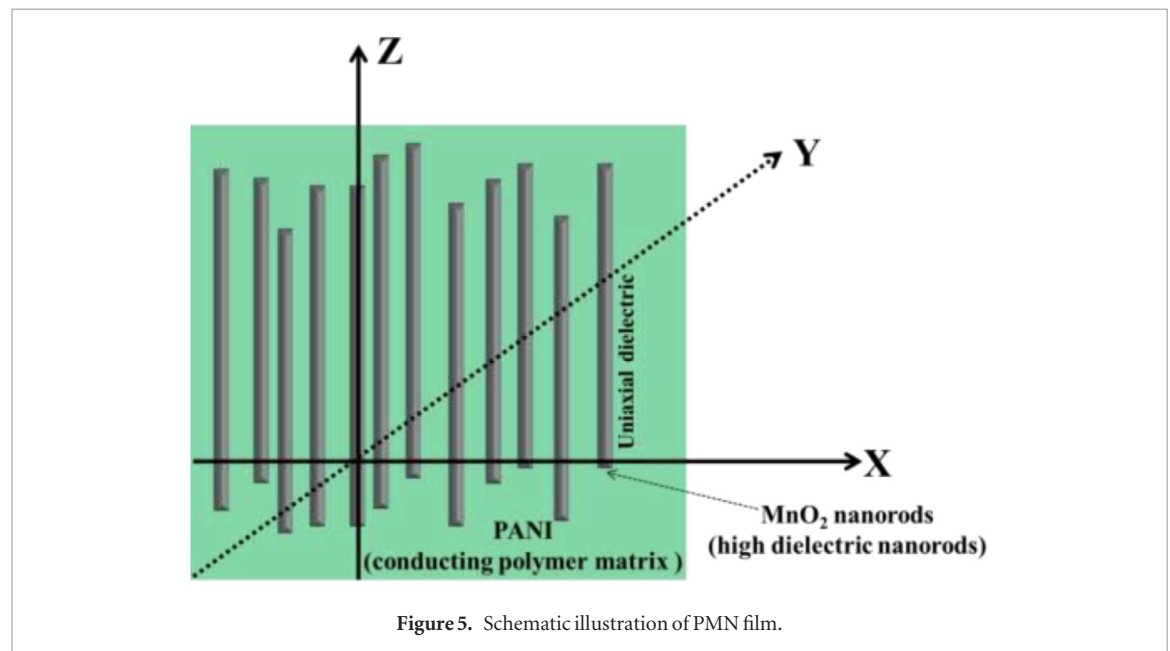Where, $A_{\text{eff}} = (1 - R - T)/(1 - R)$ is the effective absorbance of the materials and

$$\text{SE}_{\text{M}}(\text{dB}) = -20\log(1 - 10^{-\text{SE}_A/10}) \tag{4}$$

The contribution of SE$_M$ to the total EMI SE can be neglected if SE ~ 10 dB [13]. The obtained EMI SE of prepared PMN films in the X-band (8.2–12.4 GHz) were shown in figure 3(a). The effective EMI SE ~ 35 dB was obtained for 169 ± 3 μm thicker PMN film in the X-band. The SE$_A$ value of this film was found to be ~24 dB and corresponding SE$_R$ was ~11 dB (figure 3(b)). At high frequency, Ku-band (12.4–18 GHz), the most effective EMI SE of this PMN film reaches ~39 dB (figure 4(a)). The corresponding EMI SE$_A$ and SE$_R$ values were obtained ~29 dB and ~10 dB respectively (figure 4(b)). For most of the practical applications, ~20 dB EMI SE is considered as an optimum level. This can be easily achieved by using PMN film at minimum coating thickness. For 81 ± 3 μm thicker PMN film shows effective EMI SE ~ 28–24 dB (SE$_A$ ~ 18–16 dB and SE$_R$ ~ 10–8 dB) and ~26 dB (SE$_A$ ~ 17 dB and SE$_R$ ~ 9 dB) in X-band and Ku-band respectively (figures 3 and 4). Thus, the observed EMI shielding results suggests that the contribution of EMI shielding due to absorption is intrinsically dominant in the PMN film. The observed EMI SE of PMN film was compared with recently developed materials and films in the table 1.

As synthesized α-MnO$_2$ nanorods show excellent electromagnetic wave absorption property at high frequency especially in 8–18 GHz due to high dielectric loss [16]. The incident electromagnetic wave generates an electric field over the conducting PMN composite surface opposite to applied field. The high electrical loss (dissipation current) takes place along the PANI grafted MnO$_2$ nanorods and high EM attenuation loss takes place in PMN film and shows excellent EMI SE (SE$_A$). The present PMN system is a hybrid polymer nanocomposite where dielectric MnO$_2$ nanorods were dispersed. Therefore, effective permittivity also plays a key role of enhancing EMI shielding through absorption. The incident electromagnetic wave falls perpendicularly to the PANI-MnO$_2$ nanorod medium and electric field polarization takes place along the MnO$_2$ nanorods. As shown in figure 5, the MnO$_2$ nanorods can be considered as an uniaxial dielectric. As the host matrix is conducting polymer (PANI), interactions of extraordinary

Table 1. A comparison of the average total EMI SE, shielding due to absorption (SE$_A$) and shielding due to reflection (SE$_R$) of various reported materials with present work under optimal conditions.

Material	Filler loading (wt%)/ratio	Frequency (GHz)	SE (dB)	SE$_A$ (dB)	SE$_R$ (dB)	Thickness	Reff
PANI–nano-Mn$_{0.2}$Ni$_{0.4}$Zn$_{0.4}$Fe$_2$O$_4$	20:80	8.2–12.4	~50	~49–47	~1–3	2.5 mm	[36]
PANI–Mn$_{0.5}$Zn$_{0.5}$Fe$_2$O$_4$	Aniline:filler 3:2	8.2–12.4	~36	~31	~5	2 mm	[37]
PU-PANI	PU:aniline 1:1	8.2–12.4	~10			1.9 mm	[12]
Polystyrene/PANI-CNT	30 wt%	12.4–18	~24	~18	~6	1 mm	[13]
PVB/PANI nanofiber	10 wt%	8.2–12.4	~26	~21	~5	0.78 ± 0.02 mm	[34]
		12.4–18	~30	~26	~4		
PANI ES	–	0.5–13.5	~18	~12	~6	90 μm	[14]
PANI/Co-FAC	–	12.4–18	~30	~28	~2	89 ± 3 μm	[35]
PVB/PANI-Ni-FAC	10 wt%	8.2–12.4	~23	~20	~3	259 ± 2 μm	[4]
Screen printed PANI nanofiber	–	8.2–18	~13	~10	~3	50 μm	[38]
Screen printed graphene-PANI nanofiber	Aniline: filler 4:1	8.2–18	~17	~12	~5	50 μm	[38]
Paraffin wax/β-MnO$_2$ nanorods	30 wt%	8.2–12.4	~21–22	~16.5–18	~5–4	2 mm	[25]
Graphene nanoribbons /α-MnO$_2$	53 wt%	12.4–18	~11	~8.6	~2.4	0.5 mm	[41]
Paraffin/MnOOH@CNT	1:1	8–18	~13–18	~9–14	~4–3	2 mm	[42]
PANI-MnO$_2$ nanorods	Aniline:MnO$_2$ nanorod 4:1	8.2–12.4	~35	~24	~11	169 ± 3 μm	This work
		12.4–18	~28–24	~18–16	~10–8	81 ± 3 μm	
			~39	~29	~10	169 ± 3 μm	
			~26	~17	~9	81 ± 3 μm	

Figure 5. Schematic illustration of PMN film.

plane waves ($E_Z \neq 0$) with wave vector $(q_x, q_y, q_z)^T$ is high [39]. Here, phase constant (q_z) is along the Z-axis. Therefore electric field (E_z) can be expressed as (Helmholtz equation),

$$\left\{ \frac{\partial}{\partial x^2} + \frac{\partial}{\partial y^2} + (k^2 - q_z^2) \right\} E_z = 0$$

with the boundary condition $E_z = 0$ on the MnO$_2$ nanorods. According to the literature [39], it should possess a very strong spatial dispersion effect at microwave frequency which results in the enhancement of effective permittivity and EMI shielding [39].

The incident electromagnetic wave propagates through a material by changing its time average power [40] i.e. $P_{av} = \frac{1}{2} \int (E \times H^*) dS$ (where E is the electric field value and H is the associated magnetic field value, asterisk
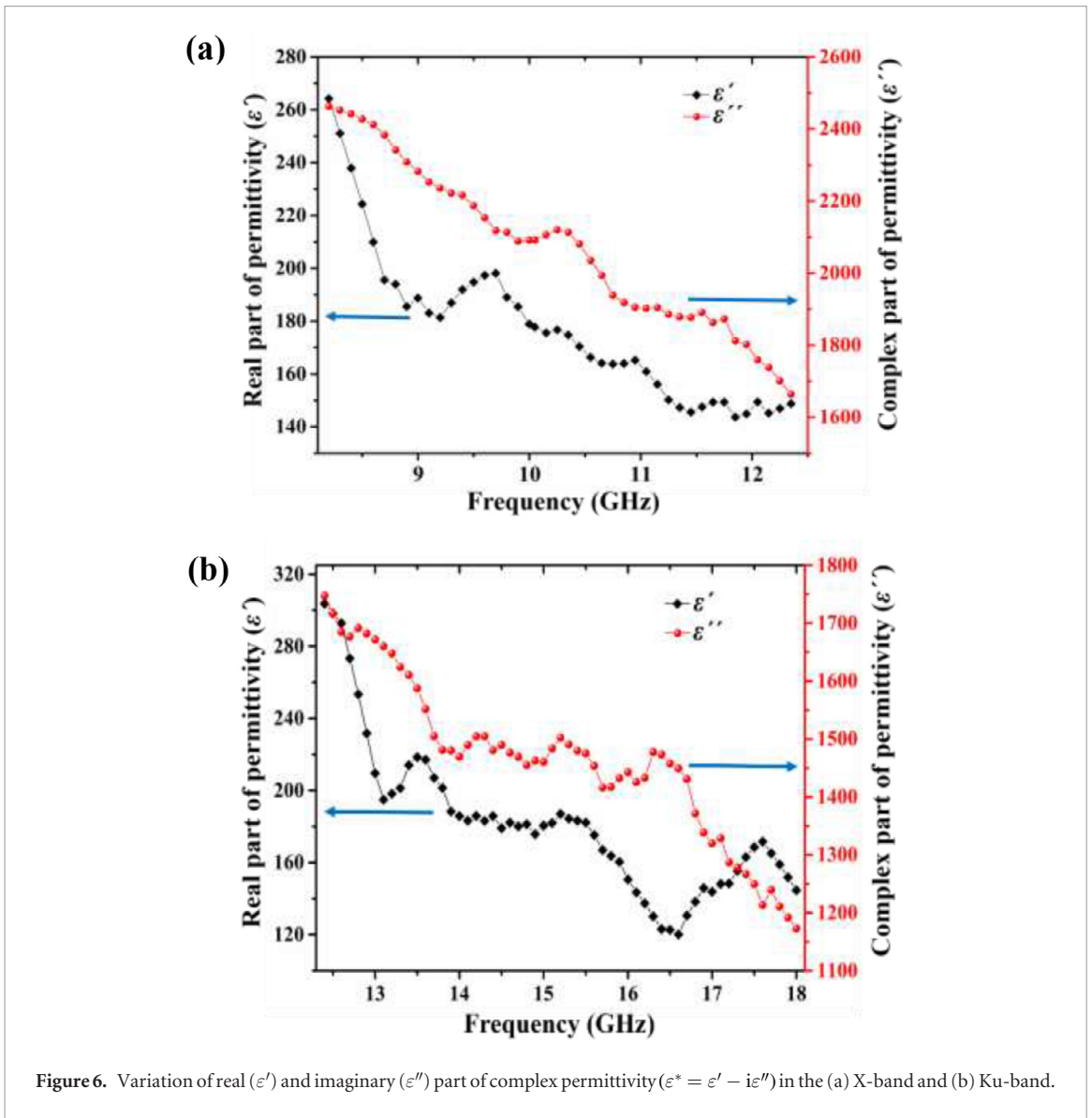
Figure 6. Variation of real (ε') and imaginary (ε'') part of complex permittivity ($\varepsilon^* = \varepsilon' - i\varepsilon''$) in the (a) X-band and (b) Ku-band.
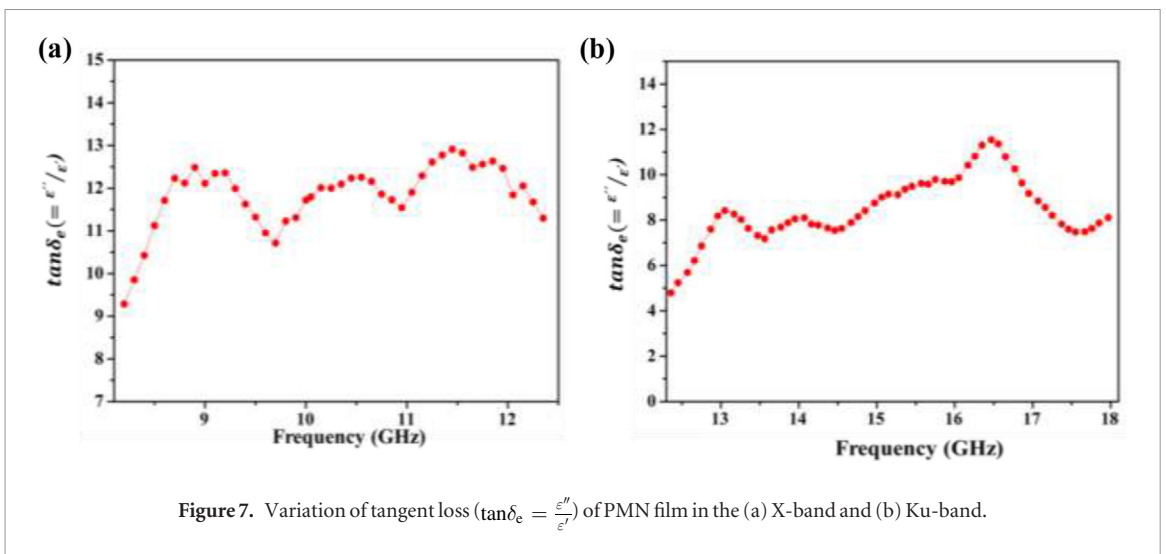

Figure 7. Variation of tangent loss ($\tan\delta_e = \frac{\varepsilon''}{\varepsilon'}$) of PMN film in the (a) X-band and (b) Ku-band.
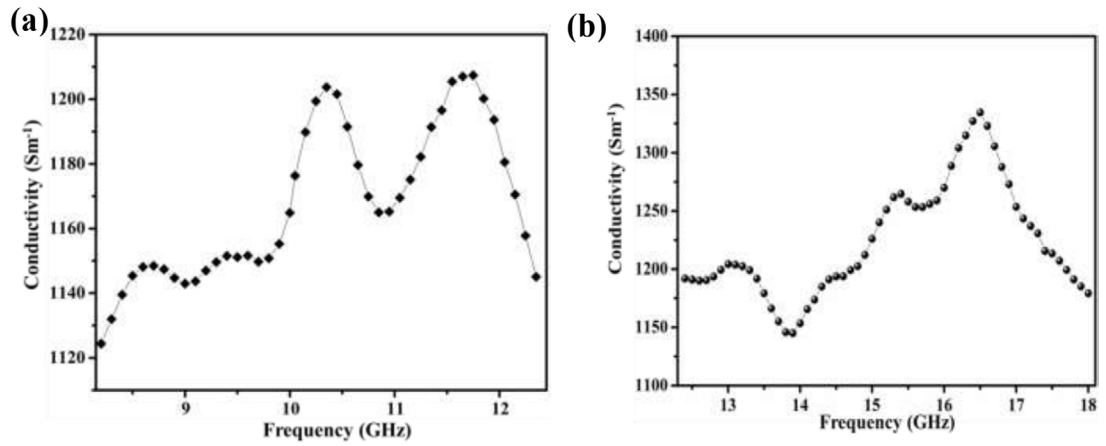
Figure 8. Variation of shield conductivity of the PMN film in the (a) X-band and (b) Ku-band.
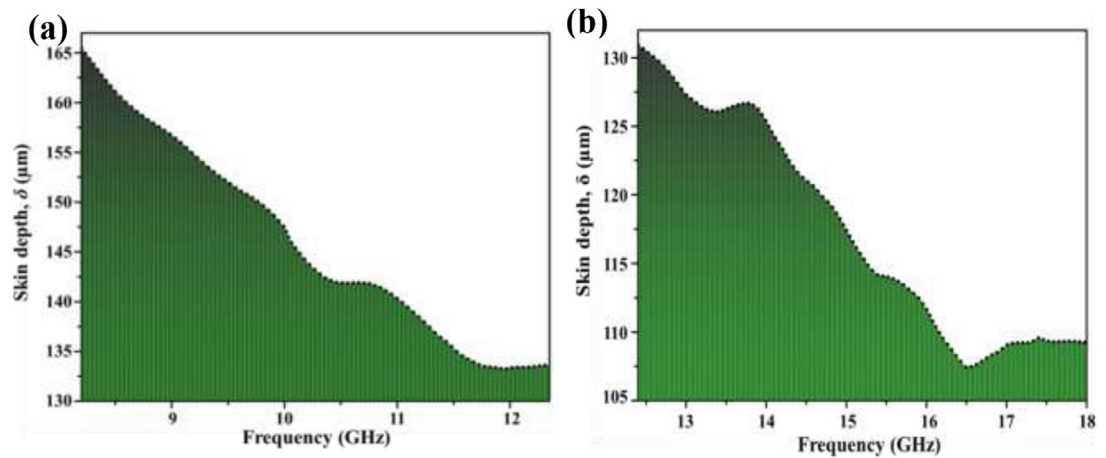

Figure 9. Variation of skin depth (penetration depth, δ) of the PMN film in the (a) X-band and (b) Ku-band.

indicates complex conjugate and it travels by exponentially decreasing its magnitude) and for an electrically thick conductor, SE_R and SE_A can be expressed as [1, 2, 40],

$$SE_R(dB) = -10\log\left\{\frac{(1-R)}{16\omega\varepsilon_\circ\mu'}\right\} \tag{5}$$

$$SE_A(dB) = -20\frac{t}{\delta}\log e = -8.68t\left(\frac{\sigma_s\omega\mu'}{2}\right)^{\frac{1}{2}} \tag{6}$$

$\omega = 2\pi f$, is the angular frequency, $\varepsilon_\circ$ is the permittivity of free space (8.854×10^{-12} Fm^{-1}), t is the thickness of the shield and δ is the skin depth (penetration depth) of the shield $(\delta) = \sqrt{2/\mu_0\mu'\omega\sigma_s}$ [1, 2, 40]. Here, μ_0 is the permeability of free space ($4\pi \times 10^{-12}$ H) and $\sigma_s = \omega\varepsilon_\circ\varepsilon''$ is the frequency dependent shield conductivity. The variation of real (ε', corresponding to polarization and storage capability of electric energy) and imaginary (ε'', corresponding to electric loss or dissipation of electric energy) parts of complex permittivity ($\varepsilon^* = \varepsilon' - i\varepsilon''$) of PMN film in the X-band and Ku-band is shown in figures 6(a) and (b), respectively. It was observed that both ε' and ε'' decrease with frequency. In X-band, ε' was found to be 270–250 whereas it was observed to be 297–200 in Ku-band. Similarly, ε'' was found to be 2490–1790 and 1793–1300 in the X-band and Ku-band, respectively. The variation of tangent loss ($\tan\delta_e = \varepsilon''/\varepsilon'$) of the PMN film in the X-band and Ku-band is shown in figures 7(a) and (b), respectively. The $\tan\delta_e$ value of PMN film was found to be 9–13 and 5–12 respectively in the X-band and Ku-band. As MnO_2 nanorods have high dielectric loss and microwave absorption property, the observed high $\tan\delta_e$ of PMN film is due to presence of MnO_2 nanorods in PANI matrix. Figures 8(a) and (b) shows the variation of shield conductivity of the PMN film in the X-band and Ku-band, respectively. The σ_s value of PMN film was found to be 1125–1201 S m^{-1} in the X-band that increased to 1192–1338 S m^{-1} in the Ku-band (figure 8(b)). The correlated barrier hopping of charge takes place over the PANI grafted MnO_2 nanorods and thus dielectric loss and shield conductivity was found to be high for PMN film.
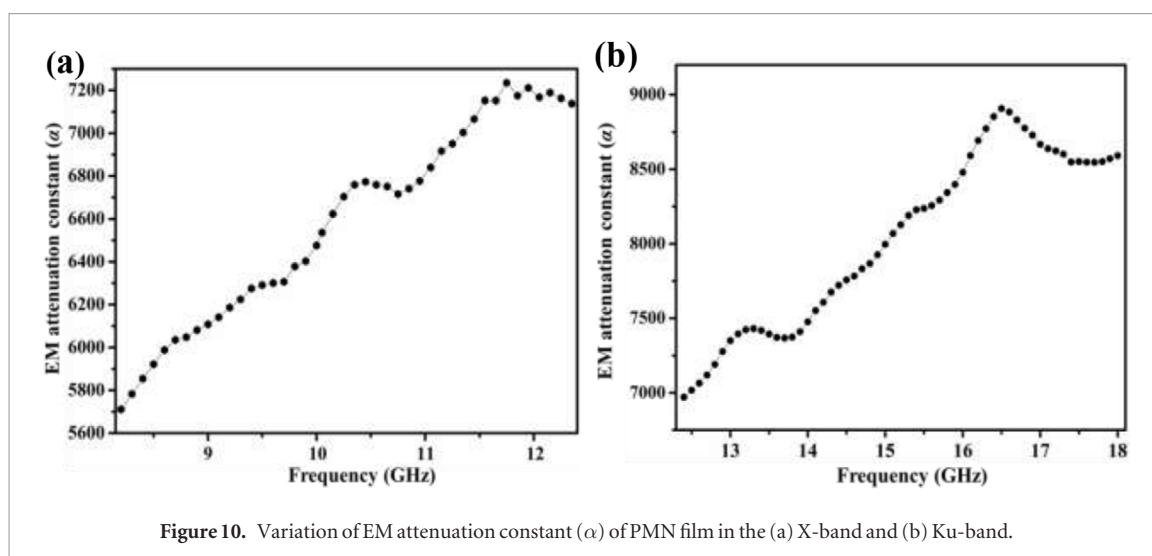
Figure 10. Variation of EM attenuation constant (α) of PMN film in the (a) X-band and (b) Ku-band.

Figures 9(a) and (b) shows the variation of skin depth (penetration depth) of the PMN film in the X-band and Ku-band respectively. The calculated skin depth of PMN film was found to be ~165 μm at 8.2 GHz which exponentially decreased to ~133 μm (at 12.4 GHz). Similarly, in the Ku-band, δ value also exponentially decreases from ~133 μm to ~105 μm (figure 9(b)).

According to the transmission line theory, the real part of the propagation constant (γ_s) $\gamma_s = \sqrt{j\omega\mu_s\sigma_s}$ gives the EM attenuation of incident electromagnetic wave [2]. The equation of EM attenuation constant (α) is [34]

$$\alpha = \frac{\sqrt{2}\,\pi f}{c} \times \left[(\mu''\varepsilon'' - \mu'\varepsilon') + \{(\mu''\varepsilon'' - \mu'\varepsilon')^2 + (\mu'\varepsilon'' + \mu''\varepsilon')^2 \}^{\frac{1}{2}} \right]^{\frac{1}{2}} \tag{7}$$

For conducting polymers and its composite films, the EM attenuation constant is the intrinsically dominant factor for EMI shielding as it depends on both ε' and ε''. Variation of α value of PMN film in X-band and Ku-band is shown in figures 10(a) and (b) respectively. In the X-band, the obtained α value of PMN film was 5698–7230 that increased to 7000–8900 in the Ku-band. Thus it suggests the excellent EM attenuation loss and EMI shielding property (SE$_A$) of PMN film in the X-band and Ku-band.

4. Conclusions

The *in situ* synthesis of PANI-MnO$_2$ nanorods composite (PMN) was carried out at $-30 \pm 2\,°C$ and free standing films were prepared by solution processing. EMI shielding property of the prepared PMN films was studied in the X-band and Ku-band frequency range. An excellent EMI SE was observed for PMN films in both the frequency bands. In X-band, ~35 dB (169 $\pm$ 3 μm) and ~26 dB (81 $\pm$ 3 μm) EMI SE was obtained for PMN film and that was increased to ~39 dB and ~27 dB in the Ku band. EMI shielding due to absorption of PMN film was found to be dominant for both bands. Further, enhancement of shield conductivity and EM attenuation constant of the PMN film also bolsters the excellent EMI shielding property.

Acknowledgments

References

[1] Tong X C 2008 *Advanced Materials and Design for Electromagnetic Interference Shielding* (Boca Raton, FL: CRC Press)

[2] Gooch J W and Daher J K 2007 *Electromagnetic Shielding and Corrosion Protection for Aerospace Vehicles* (Berlin: Springer) (http://link.springer.com/10.1007/978-0-387-46096-3 (accessed: 29 November 2015))

[3] Gedler G, Antunes M, Velasco J I and Ozisik R 2016 Enhanced electromagnetic interference shielding effectiveness of polycarbonate/graphene nanocomposites foamed via 1-step supercritical carbon dioxide process *Mater. Des.* **90** 906–14

[4] Bora P J, Mallik N, Ramamurthy P C, Kishore and Madras G 2016 Poly(vinyl butyral)-polyaniline-magnetically functionalized fly ash cenosphere composite film for electromagnetic interference shielding *Composites, Part B* **106** 224–33

[5] Liu X, Zhang L, Yin X, Ye F, Liu Y and Cheng L 2016 Flexible thin SiC fiber fabrics using carbon nanotube modification for improving electromagnetic shielding properties *Mater. Des.* **104** 68–75

[6] Joo J and Epstein A J 1994 Electromagnetic radiation shielding by intrinsically conducting polymers *Appl. Phys. Lett.* **65** 2278–80

[7] Joo J and Lee C Y 2000 High frequency electromagnetic interference shielding response of mixtures and multilayer films based on conducting polymers *J. Appl. Phys.* **88** 513–8

[8] Mohan R R, Varma S J and Faisal M and Jayalekshm S 2014 Polyaniline/graphene hybrid film as an effective broadband electromagnetic shield *RSC Adv.* **5** 5917–23

[9] Yuan B, Yu L, Sheng L, An K and Zhao X 2012 Comparison of electromagnetic interference shielding properties between single-wall carbon nanotube and graphene sheet/polyaniline composites *J. Phys. D: Appl. Phys.* **45** 235108

[10] Yuping D, Shunhua L and Hongtao G 2005 Investigation of electrical conductivity and electromagnetic shielding effectiveness of polyaniline composite *Sci. Technol. Adv. Mater.* **6** 513

[11] Fang F, Li Y-Q, Xiao H-M, Hu N and Fu S-Y 2016 Layer-structured silver nanowire/polyaniline composite film as a high performance X-band EMI shielding material *J. Mater. Chem.* C **4** 4193–203

[12] Lakshmi K, John H, Mathew K T, Joseph R and George K E 2009 Microwave absorption, reflection and EMI shielding of PU–PANI composite *Acta Mater.* **57** 371–5

[13] Saini P, Choudhary V, Singh B P, Mathur R B and Dhawan S K 2011 Enhanced microwave absorption behavior of polyaniline-CNT/polystyrene blend in 12.4–18.0 GHz range *Synth. Met.* **161** 1522–6

[14] Hong Y K, Lee C Y, Jeong C K, Lee D E and Kim K, Joo J 2003 Method and apparatus to measure electromagnetic interference shielding efficiency and its shielding characteristics in broadband frequency ranges *Rev. Sci. Instrum.* **74** 1098–102

[15] Wang Y, Guan H, Du S and Wang Y 2015 A facile hydrothermal synthesis of MnO_2 nanorod–reduced graphene oxide nanocomposites possessing excellent microwave absorption properties *RSC Adv.* **5** 88979–88

[16] Lv H, Ji G, Liu W, Zhang H and Du Y 2015 Achieving hierarchical hollow carbon@Fe@Fe_3O_4 nanospheres with superior microwave absorption properties and lightweight features *J. Mater. Chem.* C **3** 10232–41

[17] Zhuo R F, Qiao L, Feng H T, Chen J T, Yan D, Wu Z G and Yan P X 2008 Microwave absorption properties and the isotropic antenna mechanism of ZnO nanotrees *J. Appl. Phys.* **104** 094101

[18] Débart A, Paterson A J, Bao J and Bruce P G 2008 α-MnO_2 Nanowires: a catalyst for the O_2 electrode in rechargeable lithium batteries *Angew. Chem., Int. Ed.* **47** 4521–4

[19] Cheng F, Su Y, Liang J, Tao Z and Chen J 2010 MnO_2-Based nanostructures as catalysts for electrochemical oxygen reduction in alkaline media *Chem. Mater.* **22** 898–905

[20] Schlesier K, Harwat M, Böhm V and Bitsch R 2002 Assessment of antioxidant activity by using different *in vitro* methods *Free Radic. Res.* **36** 177–87

[21] Zhang H, Chen W-R and Huang C-H 2008 Kinetic modeling of oxidation of antibacterial agents by manganese oxide *Environ. Sci. Technol.* **42** 5548–54

[22] Huang M, Li F, Dong F, Zhang Y X and Zhang L L 2015 MnO_2-based nanostructures for high-performance supercapacitors *J. Mater. Chem.* A **3** 21380–423

[23] She W, Bi H, Wen Z, Liu Q, Zhao X, Zhang J and Che R 2016 Tunable microwave absorption frequency by aspect ratio of hollow polydopamine@α-MnO_2 microspindles studied by electron holography *ACS Appl. Mater. Interfaces* **8** 9782–9

[24] Guan H, Chen G, Zhang S and Wang Y 2010 Microwave absorption characteristics of manganese dioxide with different crystalline phase and nanostructures *Mater. Chem. Phys.* **124** 639–45

[25] Song W-L, Cao M-S, Qiao B-B, Hou Z-L, Lu M-M, Wang C-Y, Yuan J, Liu D-N and Fan L-Z 2014 Nano-scale and micron-scale manganese dioxide vs corresponding paraffin composites for electromagnetic interference shielding and microwave absorption *Mater. Res. Bull.* **51** 277–86

[26] Guan H, Xie J, Chen G and Wang Y 2014 Facile synthesis of α-MnO_2 nanorods at low temperature and their microwave absorption properties *Mater. Chem. Phys.* **143** 1061–8

[27] Ballav N 2004 High-conducting polyaniline via oxidative polymerization of aniline by MnO_2, PbO_2 and NH_4VO_3 *Mater. Lett.* **58** 3257–60

[28] Ramamurthy P C, Mallya A N, Joseph A, Harrell W R and Gregory R V 2012 Synthesis and characterization of high molecular weight polyaniline for organic electronic applications *Polym. Eng. Sci.* **52** 1821–30

[29] Jaidev, Jafri R I, Mishra A K and Ramaprabhu S 2011 Polyaniline–MnO_2 nanotube hybrid nanocomposite as supercapacitor electrode material in acidic electrolyte *J. Mater. Chem.* **21** 17601–5

[30] Gemeay A H, Mansour I A, El-Sharkawy R G and Zaki A B 2005 Preparation and characterization of polyaniline/manganese dioxide composites via oxidative polymerization: Effect of acids *Eur. Polym. J.* **41** 2575–83

[31] Bisanha L D, Moraes S R and Motheo A J 2010 Influence of reaction conditions on synthesis of PAni/MnO_2 composites *Mol. Cryst. Liq. Cryst.* **522** 97/[397]–104/[404]

[32] Chen L F, Ong C K, Neo C P, Varadan V V and Varadan V K 2004 *Microwave Electronics: Measurement and Materials Characterization* (New York: Wiley)

[33] Yang Y, Gupta M C, Dudley K L and Lawrence R W 2005 Novel carbon nanotube–polystyrene foam composites for electromagnetic interference shielding *Nano Lett.* **5** 2131–4

[34] Bora P J, Lakhani G, Ramamurthy P C and Madras G 2016 Outstanding electromagnetic interference shielding effectiveness of polyvinylbutyral–polyaniline nanocomposite film *RSC Adv.* **6** 79058–65

[35] Bora P J, Vinoy K J, Ramamurthy P C, Kishore and Madras G 2016 Lightweight polyaniline-cobalt coated fly ash cenosphere composite film for electromagnetic interference shielding *Electron. Mater. Lett.* **12** 603–9

[36] Gairola S P, Verma V, Kumar L, Dar M A, Annapoorni S and Kotnala R K 2010 Enhanced microwave absorption properties in polyaniline and nano-ferrite composite in X-band *Synth. Met.* **160** 2315–8

[37] Dar M A, Kotnala R K, Verma V, Shah J, Siddiqui W A and Alam M 2012 High magneto-crystalline anisotropic core–shell structured $Mn_{0.5}Zn_{0.5}Fe_2O_4$/polyaniline nanocomposites prepared by *in situ* emulsion polymerization *J. Phys. Chem.* C **116** 5277–87

[38] Joseph N, Varghese J and Sebastian M T 2016 A facile formulation and excellent electromagnetic absorption of room temperature curable polyaniline nanofiber based inks *J. Mater. Chem.* C **4** 999–1008

[39] Belov P A, Marqués R, Maslovski S I, Nefedov I S, Silveirinha M, Simovski C R and Tretyakov S A 2003 Strong spatial dispersion in wire media in the very large wavelength limit *Phys. Rev.* B **67** 113103

[40] Grimes C A and Grimes D M 1993 A brief discussion of EMI shielding materials *IEEE Aerospace Applications Conf. 1993 Digest* pp 217–26

[41] Gupta T K, Singh B P, Singh V N, Teotia S, Singh A P, Elizabeth I, Dhakate S R and Dhawan S K, Mathur R B 2014 MnO_2 decorated graphene nanoribbons with superior permittivity and excellent microwave shielding properties *J. Mater. Chem.* A **2** 4256–63

[42] Zhang Z, Dang W, Dong C, Chen G, Wang Y and Guan H 2016 Facile synthesis of core–shell carbon nanotubes@MnOOH nanocomposites with remarkable dielectric loss and electromagnetic shielding properties *RSC Adv.* **6** 90002–9